Chemical Engineering Science 163 (2017) 137–144

Contents lists available at ScienceDirect

Chemical Engineering Science

journal homepage: www.elsevier.com/locate/ces

Profile of huge wave in gas–liquid churn flow

Ke Wang [a,b], Jing Ye [c], Bofeng Bai [b,*]

[a] Beijing Key Laboratory of Process Fluid Filtration and Separation, College of Mechanical and Transportation Engineering, China University of Petroleum, Beijing 102249, China
[b] State Key Laboratory of Multiphase Flow in Power Engineering, Xi'an Jiaotong University, Shaanxi 710049, China
[c] Shanghai Marine Diesel Engine Research Institute, Shanghai 201108, China

HIGHLIGHTS

- We proposed a normal-distribution function to describe the huge wave shape.
- We analyzed the relationship between the wave amplitude and wavelength.
- The normal-distribution function reproduces the evolution of the huge wave quite well.
- The sinusoidal function comparatively has the lowest precision in prediction.
- The hemispherical function is recommended to simplify the calculation.

ARTICLE INFO

Article history:
Received 20 September 2016
Received in revised form 15 December 2016
Accepted 18 January 2017
Available online 19 January 2017

Keywords:
Churn flow
Wave profile
Huge wave
Flooding
Mathematical modeling

ABSTRACT

The knowledge of wave profile of the huge waves is crucial for the thorough study on the pressure drop in churn flow, which is of great interest in many industries where such chaotic flow occurs. The literature lacks information on the profile of a huge wave under churn flow condition. Usually, hemispherical and sinusoidal shapes are employed to feature the general characteristic of the huge wave. No doubt, errors will be inevitably result. To explore this issue, we used a high-speed camera to capture a more detailed description of the huge wave in a 19 mm i.d. tube under churn flow condition. The experimental results indicate that the ratio between wave length and wave amplitude is found to be about 5 irrespective of gas and liquid velocities. By analyzing the silhouette of the huge wave at its critical condition (stationary), we proposed a Gaussian function to describe such wave shape more accurately. Compared with the existing wave shapes, the Gaussian function qualitatively and quantitatively reproduces the evolution of the huge wave quite well whereas the sinusoidal function comparatively has the lowest precision in prediction. Though a far cry from the real wave shape, the hemispherical function is recommended to simplify the calculation on the basis of a simpler form but a sufficient accuracy.

1. Introduction

The pressure drop is of great concern for any industrial process design which in turn depends strongly on better understanding of the flow patterns. Recently, the significance of churn flow has been increasingly emphasized. This distinctive flow pattern is generally characterized by the presence of a very thick and unstable liquid film with the liquid frequently oscillating up and down (Hewitt and Hall-Taylor, 1970; Jayanti and Hewitt, 1992; Barbosa et al., 2002; Wang et al., 2013a; van Nimwegen et al., 2015; Parsi et al., 2016), leading to a violent fluctuation of the pressure gradient in the churn flow (Owen, 1986; Waltrich et al., 2013). This may cause the damage to the equipment and is of great interest in many industries where such oscillating flow occurs. Examples include applications such as gas lift in chemical engineering, emergency cooling of the reactor core in case of the loss of coolant, and potential flow pattern transition from severe slugging to churn flow in a pipeline-riser system, etc.

The existence of huge waves (or called flooding-type wave or large wave) formed on the thin falling liquid film is one of the most important features of churn flow. Previous experimental and analytical investigations on the huge wave properties have been mainly focused on the wave velocity, wave amplitude, wave frequency and its entrainment mechanism (Barbosa et al., 2002; Wang et al., 2013a; Tekavčič et al., 2016; Sharaf et al., 2016). It is noteworthy that the pressure drop in two-phase flow is largely influenced by the gas-liquid interface roughness. As in a highly-disturbed flow, huge waves with large amplitude flow up and down throughout the regime, resulting in the liquid film to act as

* Corresponding author.
E-mail address: bfbai@mail.xjtu.edu.cn (B. Bai).

http://dx.doi.org/10.1016/j.ces.2017.01.041
0009-2509/

Nomenclature

A_w	wave amplitude (m)
d_T	pipe diameter (m)
F	force (kg m s^{-2})
$\sum F$	resultant force (kg m s^{-2})
g	gravitational acceleration(m s^{-2})
Q	mass flow rate (kg s^{-1})
P	pressure (Pa)
r	radial distance (m)
Re	Reynolds number
S	area (m^2)
t	time (s)
u_{gs}	superficial gas velocity (m s^{-1})
u	velocity (m s^{-1})
V_w	wave volume (m^3)
v	wave velocity (m s^{-1})
z	axial direction

Greek symbols

ρ	density (kg m^{-3})
τ	shear stress (kg m^{-1} s^{-2})
δ	film thickness (m)
μ	viscosity (kg s^{-1} m^{-1})
λ	wavelength (m)
σ	standard deviation

Subscripts

f	liquid film
g	gas phase
l	liquid phase
w	wall, wave

a very rough wall and its roughness significantly affects the frictional component of the pressure drop (Parsi et al., 2015a,b; Sharaf et al., 2016). Evidently, the huge wave has to be described with appropriate terms concerning its shape to determine the gas-liquid interface roughness. Additionally, the modeling work of huge wave behaviors and entrainment requires the description of wave shape (Wang et al, 2012; Wang et al., 2013b). No doubt, the assumption of wave shape inevitably brings errors.

Some of the experimental work available in the literature concentrates on the wave structure of disturbance wave in annular flow (Hewitt et al., 1985; Wang et al., 2004; Han et al., 2006; Omebere-Iyari and Azzopardi, 2007; Hazuku et al., 2008). Their findings indicate that the interfacial wave more likely have a log-normal distribution. However, the literature lacks information on the profile of a huge wave under churn flow condition. Usually, the hemispherical and sinusoidal shapes are employed to feature the general characteristic of the huge wave. McQuillan et al. (1985) proposed a hemispherical shape to simplify the calculation, which was also adopted by Da Riva and Del Col (2009) and Ryua and Park (2011). Definitely, this simplification makes the calculation much easier; however, the hemispherical shape is a far cry from the real wave. Shearer and Davidson (1965) estimated the standing wave as a sinusoidal shape, which was verified by Hewitt et al. (1985). Subsequently, the sinusoidal wave widely serves as a more accurate approach for interfacial wave shape (disturbance and huge waves) in modeling works (Holowach et al., 2002; Barbosa et al., 2001; Wang et al., 2012, 2013b). However, there is no comparison of these two hypothesis and investigation of their effect on modelling accuracy. As we know, the huge wave is much larger compared to the regular disturbance wave and travels at a higher velocity. To our best known, there is a dearth of data on the profile of the huge wave under churn flow condition. Part of the reason that the wave profile has not been thoroughly investigated is due to the intricate nature of churn flow, resulting in that the interfacial wave in churn flow is quite hard to measure. Thus, it is strongly desired to have correlations that can describe the accurate profile of the huge wave.

To explore this issue, one of the objectives of this work is to obtain the profile of the huge wave under churn flow condition. We used a high-speed camera to capture a more detailed description of the huge wave. According to the experimental data, we aimed to find the relationship between wave length and wave amplitude. Based on the analysis of the generation and evolution of the huge waves under various flow conditions. We proposed a Gaussian function to describe the wave shape more accurately. By comparing the proposed profile with the existing wave shapes of hemispherical and sinusoidal in wave evolution calculations, we tried to provide insight into the effect of wave shape on the modeling accuracy. It is realized that the calculations could be quite complicated with such Gaussian wave shape. With this in mind, we compared these wave shapes with the intention of finding a simpler wave shape, but features the general characteristics of the huge wave.

2. Experimental system and method

2.1. Test facility

The schematic of the test facility is presented in Fig. 1, which is mainly composed of the test section, water and air supply systems, as well as the measurement system. The vertical test section is made of a transparent acrylic resin and with the inner diameter of 19 mm. The air was fed from the compressor via the rotameter into the test section at the bottom of the pipe, whereas the water was injected into the water inlet section via the orifice flowmeter and fed through the porous wall to form a liquid film along the pipe circumference.

It should be noted that the configuration of the water inlet section (air-water mixer) is of utmost importance for the formation of the huge waves. In order to achieve the circumferential uniform distribution of the liquid phase as that in the Taylor bubble, the water inlet section (porous wall) is delicately designed. About 300 holes of 1 mm in diameter in 15 rows with the spacing distance about 2 mm is uniformly distributed in water inlet section. Additionally, an extraction sinter was also fabricated to extract the falling film out of the tube.

The Memrecam fx K3 high-speed CCD camera with the capability of up to 10,000 frame/s was employed to capture the generation and evolution of the huge waves. In the present study, the camera was placed to face the water inlet section with the sample frequency of 1000 frame/s.

2.2. Experiment procedure and conditions

The detailed experimental procedure can be referred to our previous paper (Wang et al., 2013a). When a falling film formed along the pipe circumference at a constant liquid flow rate, the gas flow rate was subsequently increased from a lower flow rate until churn flow was obtained in the tube, showing that part of the liquid flew downwards as a falling film, whereas above the injector part of the

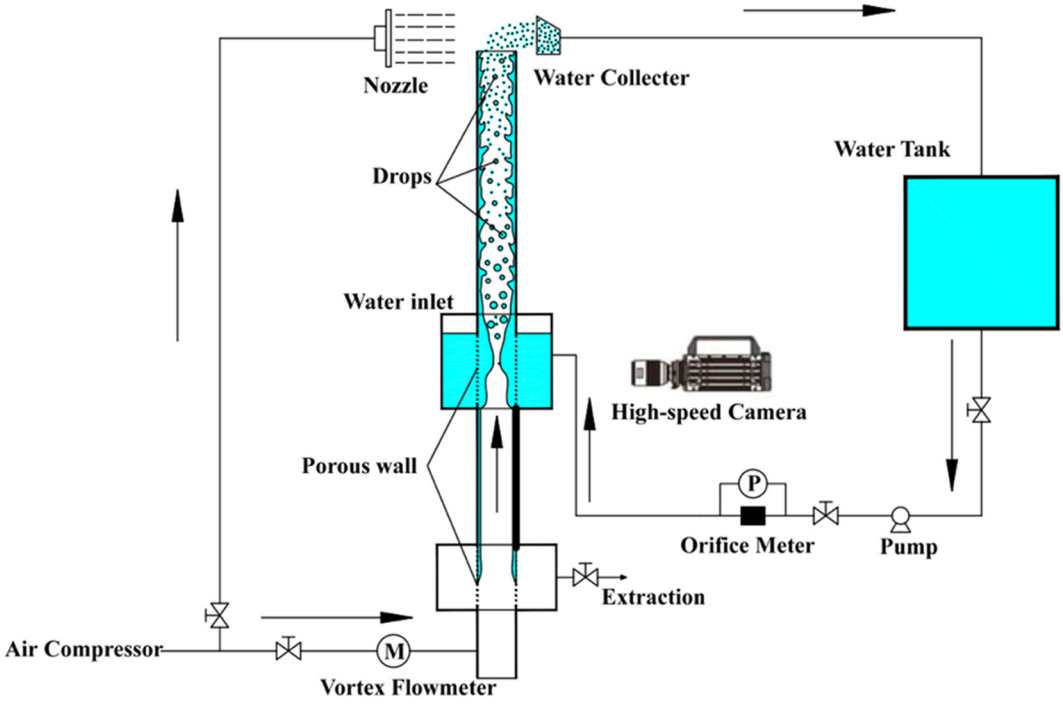

Fig. 1. Test facility.

liquid flew upwards. Remarkably, coherent huge waves were observed repeatedly formed in the region of the water inlet and transported upwards into the upper part of the pipe and eventually broke up into droplets.

All experiments were carried out under the atmospheric pressure. The data were collected under the predetermined gas and liquid flow conditions: the gas superficial velocity u_{sg} ranged from 4.90 m/s to 12.74 m/s and the liquid superficial velocity u_{sl} ranged from 5.75×10^{-2} to 8.78×10^{-1} m/s.

2.3. Data processing

In terms of wave behavior, the huge wave firstly travels downwards to the "balanced" position then reverses to travel upwards. The wave crest is commonly "undercut" or "stretched" which leads to the distortion of the wave shape. Only at the "balanced" position, the shape of the huge wave (stationary wave) remains symmetrical, providing a convenient way to access the information about the huge wave. Normally, we define this situation as a critical condition for wave reversal. Fig. 2a displays an example of an instantaneous image of the stationary wave. On the basis of white/black contrast (WBC) of the gas/liquid interface near the inner wall, it is clear enough to distinguish the wave border. Accordingly, the pixels of the wave silhouette were extracted and then mapped on the Cartesian coordinates, as seen in Fig. 2b.

2.4. Uncertainty

The water flow is measured by an orifice mass flux meter with the uncertainty of 0.5%, and the pressure drop by a Rosemount 3051 transmitter with the uncertainty of ±0.5% as well as the air flow by a rotameter whose accuracy grade attains 1.0 classes. It is should be noted that a small amount of gas randomly escapes from the water inlet and extraction sections, but the amount of the extracted gas is negligible. The measurement of huge waves under chaotic churn flow condition is a challenge, and further distortion of the wave shape and subsequent entrainment which all cause a hazy outline and impede accurate measuring of the wave profile. In the present study, we only focus on the profile of the huge wave at its critical condition, where it maintains its shape.

3. Results and discussion

3.1. Wave shape description

The liquid film is composed of the huge wave and the base film, as illustrated in Fig. 3. According to the wave silhouettes, we carefully checked the wave profiles under various flow conditions and employed a Gaussian function to describe the wave shape as:

$$\delta = \delta_b + A_w e^{-\frac{(z-z_c)^2}{2\sigma^2}} \tag{1}$$

where δ_b, A_w, z, z_c and σ are the thickness of the base film, wave amplitude, axial distance, the symmetry axis of the wave shape and the standard deviation of the Gaussian function, respectively. In the present paper, z_c is supposed to be the half of the wave length λ ($z_c = \frac{1}{2}\lambda$). Considering the standard deviation, 99% of values are found within three standard deviations of the mean [$z_c - 3\sigma$, $z_c + 3\sigma$]. The values of the wave mapped on the z axis are assumed to fit in with the distributing disciplinarian, that is, 99% of the wave values are falling in [0, λ] considering the errors in the experiment. Thus,

$$6\sigma = \lambda \Rightarrow \sigma = \frac{1}{6}\lambda \tag{2}$$

Therefore, the shape of the huge wave can be described as:

$$\delta(z) = \delta_b + A_w e^{\frac{-18(z-\frac{1}{2}\lambda)^2}{\lambda^2}} \tag{3}$$

Fig. 4 shows the relationship between the wavelength λ and wave amplitude A_w under various flow conditions. It appears that the ratio $\frac{\lambda}{A_w}$ is mostly distributed among 4 and 6, but has no obvious correlation with gas and liquid velocities. As a simplification, the ratio approximately settles as $\frac{\lambda}{A_w} \approx 5$.

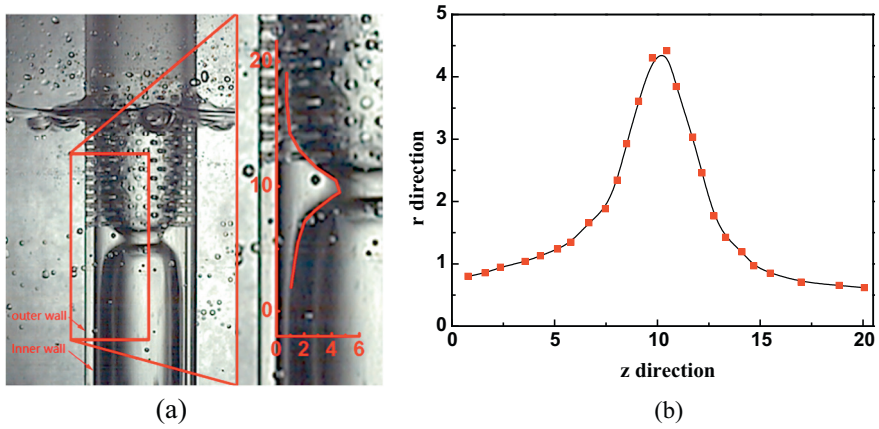

Fig. 2. Examples of instantaneous wave shape extraction. $u_{sg} = 5.98$ m/s, $Q_l = 16.25 \times 10^{-2}$ kg/s, $d_T = 19$ mm.

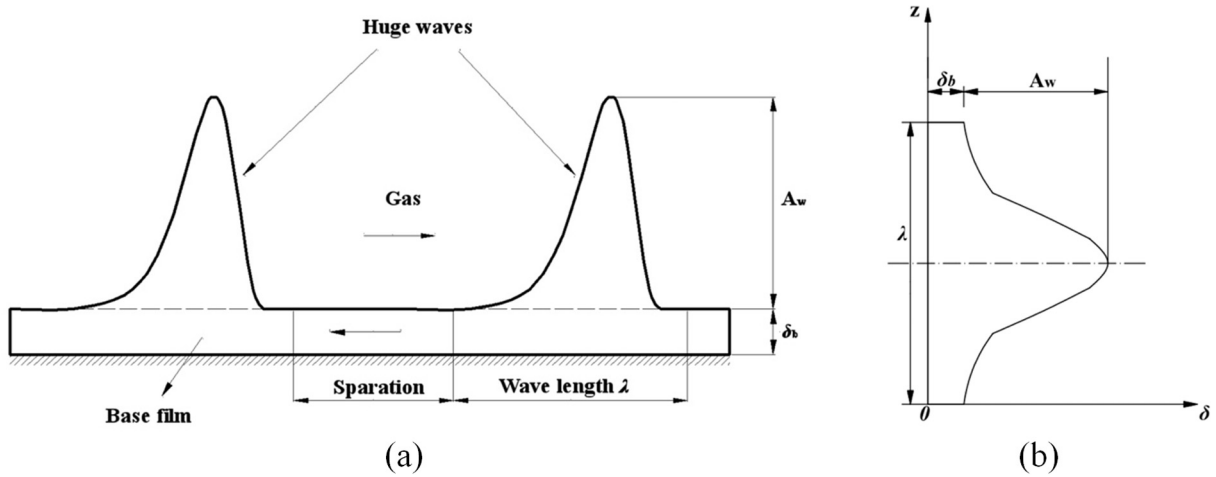

Fig. 3. Axial distribution and the shape of huge waves.

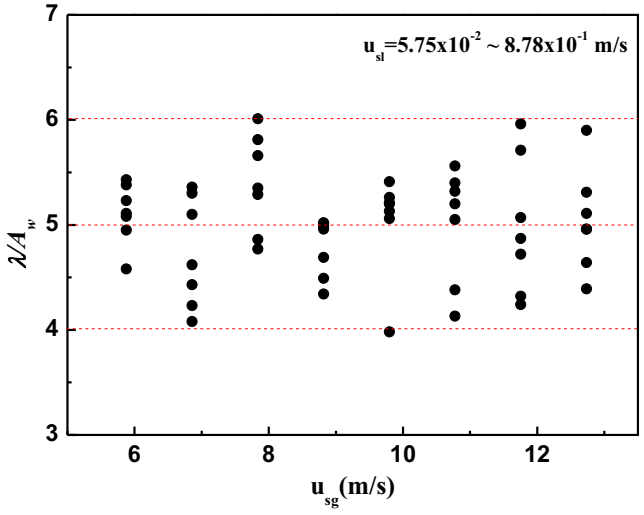

Fig. 4. the relation between the wave length λ and wave amplitude A_w.

3.2. Comparison of the proposed shape function with the existing ones

Note that Eq. (3) proposed in this paper can describe the huge wave shape well, which is also demonstrated later in Fig. 6. However, such a Gaussian function would inevitably complicate the modeling work. For a simplification, the sinusoidal shape or hemispherical shape is commonly used to describe the wave shape, as seen in Fig. 5.

The arbitrary thickness of liquid film δ in the wave region with the sinusoidal and hemispherical shape can be described respectively as follows:

$$\text{Sinusoidal shape}: \quad \delta(z) = \frac{1}{2}\left[(2\delta_b + A_w) - A_w \cos\frac{2\pi z}{\lambda}\right], \quad 0 \leqslant z \leqslant \lambda \tag{4}$$

$$\text{Hemispherical shape}: \quad \delta(z) = \delta_b + \sqrt{2A_w z - z^2}, \quad 0 \leqslant z \leqslant \lambda \tag{5}$$

Fig. 6 shows the qualitative comparison of different wave shape functions with the experiment data. Obviously, the Gaussian function fits the experiment data quite well, whereas the sinusoidal function unexpectedly goes to another extremeness especially near wave waist. For the hemispherical function, although a far cry from the real wave shape, it describes a similar volume of the wave, i.e. a similar gravity acting on the huge wave to affect the wave behavior. Additionally, we also introduced the error analysis to quantitatively verify the accuracy of the wave shape functions (see Table 1). In the present study, the root mean square error (RMSE) which describes the deviation between the fitting points and original data and the coefficient of determination (R-square) which provides the information about the goodness of fit of the function were employed. It is

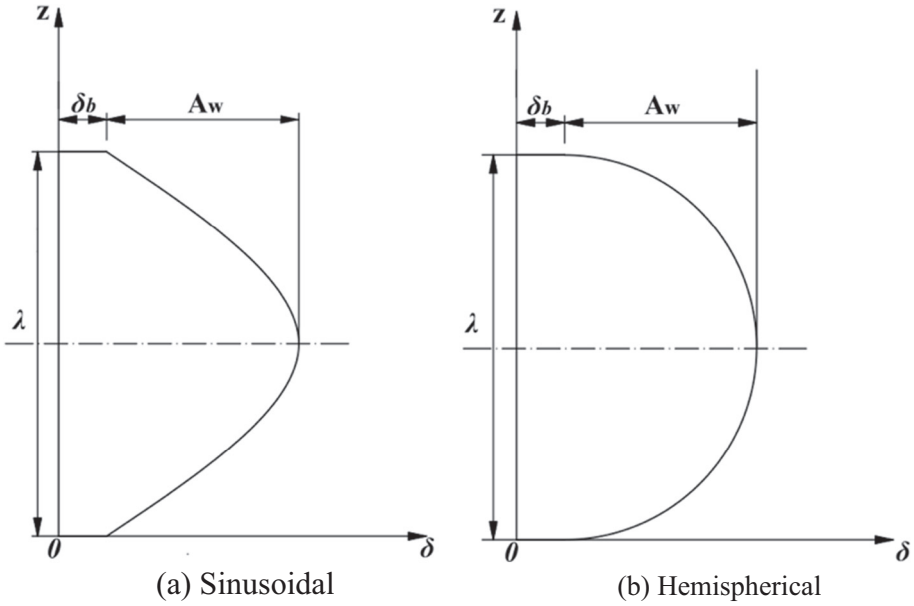

Fig. 5. Simplified wave shapes.

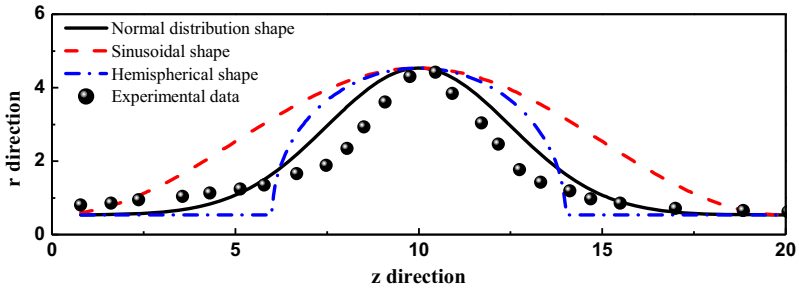

Fig. 6. Comparison between different wave shape functions.

Table 1
Error analysis of different wave shape functions vs. experimental data.

	Gaussian	Sinusoidal	Hemispherical
RMSE	0.5529	1.2980	0.9091
R-square	0.7769	−0.2294	0.3969

noted that RMSE getting close to 0 and R-square approaching 1 indicate a more accurate fitting of experimental data. Thus, in conclusion, the Gaussian function proposed here precisely features the general characteristics of the huge wave.

3.3. Verification of shape functions in wave development modeling

As mentioned earlier, since the modeling work such as pressure gradient, wave behavior and entrainment requires the appropriate description of wave shape, the impact of wave shape assumption on calculation accuracy needs sufficient attention. In the present study, we only focus on the effect of wave shape on the wave amplitude variation prediction. Evidently, the calculation could be accurate, but quite complicated with proposed Gaussian function. Meanwhile, the sinusoidal and hemispherical functions have the benefit of reducing the computational complexity even though different from the real shape. Thus, it is worth comparing these wave shapes with the intention of finding a simpler wave shape, but features the general characteristics of the huge wave in calculations of wave evolution.

The observation shows that the wave reversal occurs when the weight of the downward wave is balanced by the forces tending to cause the wave to move upward along the tube walls. In the present work, the upward gas pressure force $\vec{F}_{pc}$, the downward gravitational force $\vec{F}_g$ and the wall shear stress force $\vec{F}_{ws}$ exerted on the control volume are taken into account, as seen in Fig. 7. It should be noted that the wall shear stress force is in the opposite direction of the wave movement. Thus, the resultant force $\Sigma\vec{F}$ acting on the control volume can be described as:

$$\Sigma\vec{F} = \vec{F}_{pc} + \vec{F}_g + \vec{F}_{ws} \tag{6}$$

The gravitational force F_g can be calculated by:

$$F_{wg} = (\rho_l - \rho_g)gV_w \tag{7}$$

where ρ_l, ρ_g, g and V_w are the liquid density, gas density, the gravitational acceleration and the volume of the wave, respectively. The wave volume V_w can be estimated by:

$$V_w = \pi \int_0^{\lambda} (d_T - \delta(z))\delta(z)dz \tag{8}$$

where d_T is the pipe diameter. Thus, the wave volume with different profile functions can be obtained by integration as:

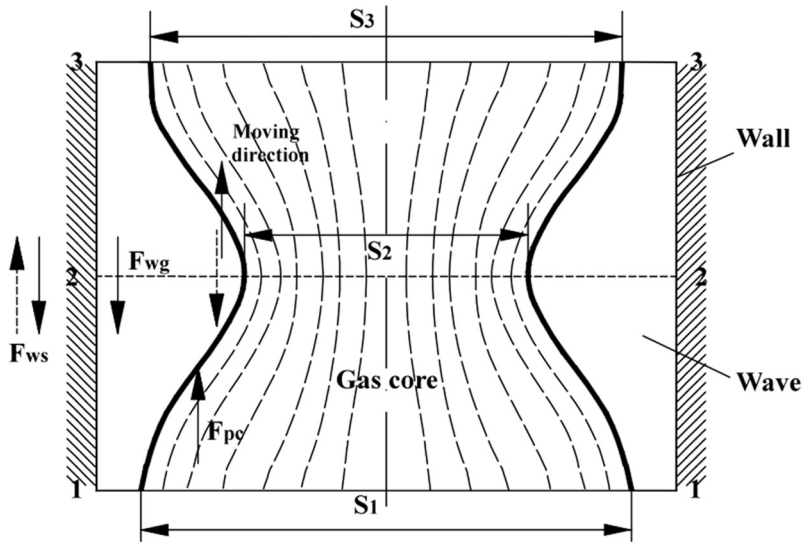

Fig. 7. The forces acting on the wave.

$$\text{Sinusoidal}: \quad V_w = \frac{5}{8}\pi A_w(4d_T A_w + 8d_T\delta_b - 3A_w^2 - 8A_w\delta_b - 8\delta_b^2) \tag{9}$$

$$\text{Hemispherical}: \quad V_w = \tfrac{1}{6}A_w\pi(3\pi d_T A_w + 12 d_T\delta_b - 8A_w^2 - 6\pi A_w\delta_b - 12\delta_b^2) \tag{10}$$

$$\begin{aligned}\text{Gaussian}: V_w &= \pi\left(\frac{5}{6}\sqrt{2\pi}\mathrm{d_T erf}\left(3\sqrt{2}/2\right)\mathrm{A_w^2} + 5\mathrm{d_T A_w}\delta_\mathrm{b} - \frac{5}{6}\sqrt{\pi}\mathrm{erf}(3)\mathrm{A_w^3}\right)\\ &\quad -\frac{5}{3}\sqrt{2\pi}erf(3\sqrt{2}/2)A_w^2\delta_b - 5A_w\delta_b^2\\ &\approx \pi(2.083 d_T A_w^2 + 5 d_T A_w\delta_b - 1.477A_w^3 - 4.166A_w^2\delta_b - 5A_w\delta_b^2)\end{aligned} \tag{11}$$

The gas pressure force F_{pc} is related to the pressure variation in the gas core ΔP_g and the wave projected area in the cross-section S_p:

$$F_{pc} = \Delta P_g S_p \tag{12}$$

$$S_p = \pi A_w(d_T - A_w) \tag{13}$$

The pressure variation in the gas core ΔP_g can be obtained by (McQuillan et al., 1985):

$$\Delta P_g = \Delta P_{1,2} + \Delta P_{2,3} \tag{14}$$

where $\Delta P_{1,2}$ and $\Delta P_{2,3}$ are the pressure difference between Sections 1-2 and Sections 2-3, respectively. $\Delta P_{1,2}$ is determined from a Bernoulli analysis of the gas phase:

$$\Delta P_{1,2} = P_1 - P_2 = \frac{1}{2}\rho_g u_g^2\left[\left(\frac{S_1}{S_2}\right)^2 - 1\right] \tag{15}$$

$$S_1 = \frac{1}{4}\pi(d_T - 2\delta_b)^2 \tag{16}$$

$$S_2 = \frac{1}{4}\pi(d_T - 2A_w)^2 \tag{17}$$

where S_1 and S_2 are the cross-sectional area for the gas flow at the wave windward and at the wave crest, respectively. $\Delta P_{2,3}$can be calculated using the momentum equation for steady flow as:

$$\Delta P_{2,3} = P_2 - P_3 = \rho_g u_g^2\left[1 - \left(\frac{S_3}{S_2}\right)\right] \tag{18}$$

where S_3 is the cross-sectional area for the gas flow at the wave leeward. It is noted that $S_1 = S_3$. Therefore, Eqs. (10) and (13) are substituted into Eq. (9) and pressure variation in the core ΔP_g can be determined by:

$$\Delta P_g = \frac{1}{2}\rho_g u_g^2\left[1 - \left(\frac{S_1}{S_2}\right)\right]^2 \tag{19}$$

According to the Nusselt film theory, the thickness of the base film δ_b can be obtained by:

$$\delta_b = \left(\frac{3\cdot Q_f\cdot\mu_l}{\pi\cdot d_T\cdot\rho_l\cdot g}\right)^{1/3} \tag{20}$$

where $Q_f$and μ_l are the mass flow rate of the falling film and liquid viscosity, respectively.

The wall shear stress force F_{ws} can be obtained as:

$$F_{ws} = \pi d_T\lambda\tau_w \tag{21}$$

$$\tau_w = \frac{1}{2}f_w\rho_l u_l^2 \tag{22}$$

where τ_w is the wall shear stress and f_w is the wall friction coefficient (Sawai et al., 2004).

$$f_w = \begin{cases}\frac{16}{Re_l} & (Re_l < 3000)\\ \frac{0.0791}{Re_l^{0.25}} & (Re_l \geqslant 3000)\end{cases} \tag{23}$$

where Re_l is the liquid film Reynolds number.

The mass and momentum conservation principles for wave development are described as:

$$\sum F = \rho_l\frac{d}{dt}(vV_w) - u_f\Delta Q_l \tag{24}$$

$$\rho_l\frac{dV_w}{dt} = \Delta Q_l \tag{25}$$

where v, u_f and ΔQ_l are the wave velocity, liquid velocity entering the control volume and the net liquid mass flow rate of entering the control volume, respectively. The wave velocity v can be calculated as:

$$v = \frac{dz}{dt} \tag{26}$$

where z is the distance that the wave travels. The increment of the liquid mass flow rate ΔQ_l can be estimated by:

$$\Delta Q_l = \rho_l(v - u_f)\pi\delta_b(2r_T - \delta_b) - Q_f \leqslant 0.9Q_l \quad (27)$$

The initial calculation condition is defined as when the resultant force acting on the control volume is equal to zero ($\Sigma F = 0$). According to the information provided by Assad et al. (1998) and Barbosa et al. (2001), the flow rate in the falling film is assumed to be $Q_f = 0.1Q_l$. For solving Eqs. (24)–(26) in time, a four-order Runge–Kutta-type numerical method is employed in the present study.

Fig. 8 depicts the formation of the huge wave and its evolution. The huge wave periodically forms at the bottom of the inlet section and grows in both the radial and axial direction. Owing to the gravity, the wave moves slightly down beyond the porous-wall section till it reaches the critical amplitude for the flow reversal (t = 0.030 s). Then it starts to travel upwards and subsequently grows to its maximum amplitude (t = 0.052). It is worthwhile to mention that part of the liquid is entrained into the gas core, and eventually breaks up into droplets of various sizes during the upward moving process. Serving as a reproduction of the wave evolution in Fig. 8, Fig. 9 describes the development of the huge wave with different shape functions. With the proposed Gaussian function, the wave reaches its maxima amplitude in the shortest time whereas it takes the longest time for wave to grow to its maxima amplitude with the sinusoidal function. Remarkably, the Gaussian function accurately reproduces the development of the wave, i. e. the time for wave reaching its critical and maxima amplitude with the Gaussian function coincides quite well with the experimental data. Besides, the hemispherical function has a fair good precision in critical condition prediction. However, the divergence is observed for the sinusoidal function.

Fig. 10 describes the ratio between the predicted wave amplitude at the critical condition and the measured results. Obviously, the calculation deviations of three functions decrease with the increase in liquid mass flow rate and this diminishing effect apparently becomes less pronounced when $Q_l \geqslant 0.0241$ kg/s. The reason is that the effect of pressure force in the liquid film apparently becomes less pronounced at higher liquid mass flow rate. Thus, the ignorance of the pressure force in the liquid film reduces the precision of prediction when the liquid mass flow rate is low. Additionally, the Gaussian function is the most accurate whereas the sinusoidal function comparatively has the lowest precision. Although quite different from the real wave shape, the

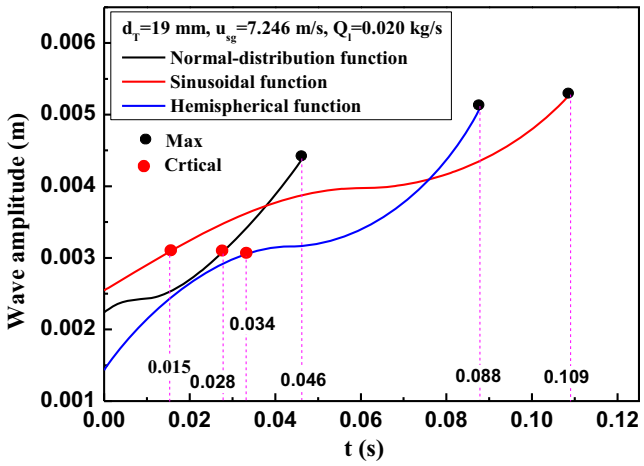

Fig. 9. Evolution of wave with three shape functions.

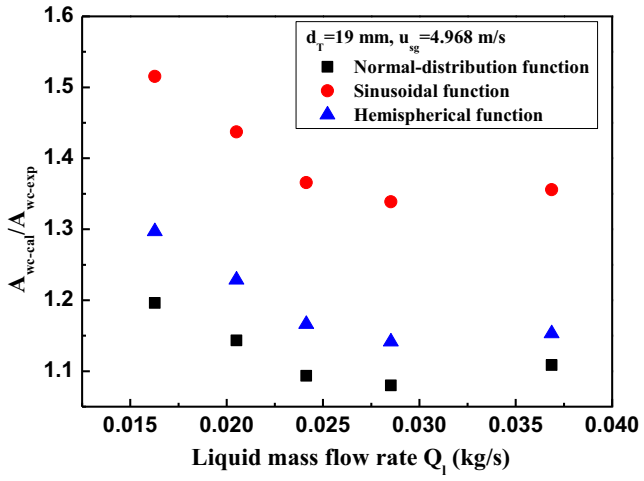

Fig. 10. Comparison of shape functions with experimental wave critical amplitude.

hemispherical function has a nearly similar accuracy with the Gaussian function. This is probably due to the fact, as mentioned before, that the gravity in hemispherical function calculation is similar as that by the Gaussian function. Fig. 11 shows the

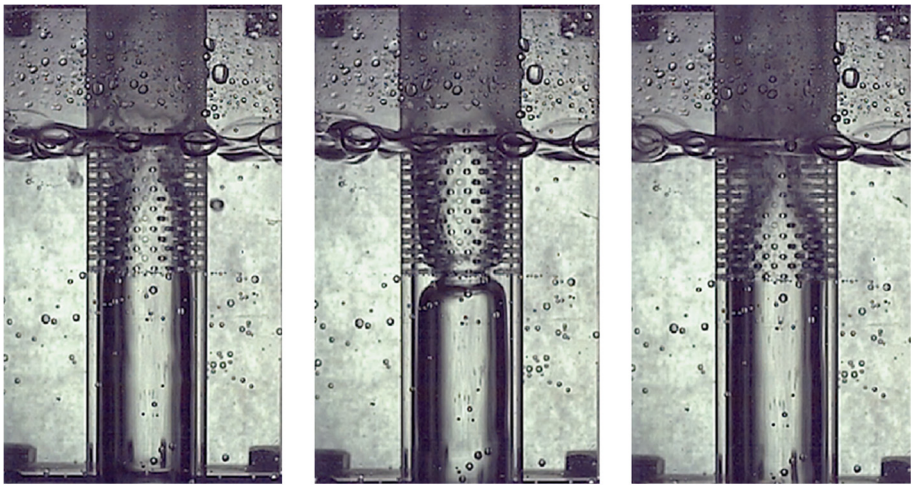

Fig. 8. Typical evolution of the huge wave (d_T = 19 mm, u_{sg} = 7.246 m/s, Q_l = 0.020 kg/s).

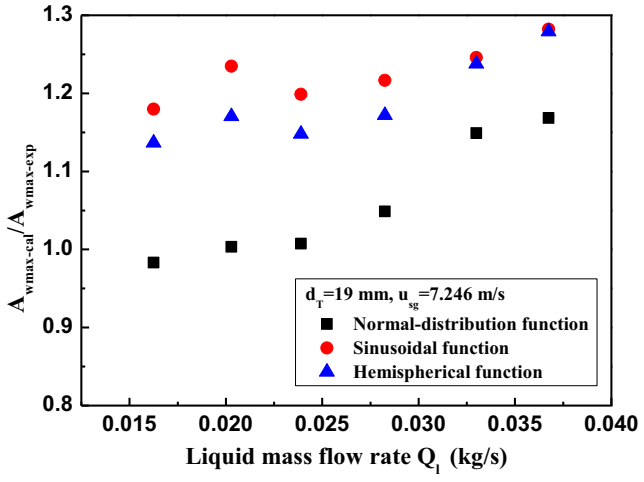

Fig. 11. Comparison of shape functions with experimental wave maxima amplitude.

prediction accuracy of wave maxima amplitude with shape functions. The prediction results with the Gaussian function coincide with the experimental data quite well for lower liquid mass flow rate whereas, for higher liquid mass flow rate, the predicted wave maxima amplitude deviates from the measured ones. This is probably due to ignorance of the effect of entrainment and wave crest distortion in the model. In addition, the hemispherical function has a similar accuracy with the sinusoidal function in wave maxima amplitude prediction.

4. Conclusions

In the present paper, we used the high-speed camera to obtain the profile of the huge wave under churn flow condition. By extracting pixels of the silhouette of the huge wave at its critical condition, a Gaussian function is proposed to describe the wave shape more accurately. Additionally, the ratio between wave length and wave amplitude is mostly distributed around 5. In order to compare the accuracy of the proposed wave profile function with the existing sinusoidal and hemispherical functions, we rebuilt the physical model for wave development based on the force analysis. Qualitatively and quantitatively compared with the experimental data, the Gaussian function successfully reproduces the wave evolution and has the highest accuracy in prediction of wave properties. Although the sinusoidal function describes the general shape of the wave and widely used, it comparatively has the lowest precision to predict the growth of the huge wave. No doubt, the hemispherical function is quite different from the real wave shape, however, it has a simpler form with a sufficient accuracy for the prediction of the general wave characteristics. Therefore, the hemispherical function is recommended to simplify the calculation.

Acknowledgments

The authors gratefully acknowledge research support from the National Natural Science Foundation of China under Grant No. 51276140, 51474229 and the Science Foundation of China University of Petroleum, Beijing No. 2462016YJRC029.

References

Assad, A., Jan, C., Lopez de Bertodano, M., Beus, S., 1998. Scaled experiments in ripple annular flow in a small tube. Nucl. Eng. Des. 184, 437–447.
Barbosa, J.R., Hewitt, G.F., König, G., et al., 2002. Liquid entrainment, droplet concentration and pressure gradient at the onset of annular flow in a vertical pipe. Int. J. Multiph. Flow 28 (6), 943–961.
Barbosa, J., Govan, A.H., Hewitt, G.F., 2001. Visualization and modeling studies of churn flow in a vertical pipe. Int. J. Multiph. Flow 27 (12), 2105–2127.
Da Riva, E., Del Col, D., 2009. Numerical simulation of churn flow in a vertical pipe. Chem. Eng. Sci. 64 (17), 3753–3765.
Han, H., Zhu, Z., Gabriel, K., 2006. A study on the effect of gas flow rate on the wave characteristics in two-phase gas–liquid annular flow. Nucl. Eng. Des. 236 (24), 2580–2588.
Hazuku, T., Takamasa, T., Matsumoto, Y., 2008. Experimental study on axial development of liquid film in vertical upward annular two-phase flow. Int. J. Multiph. Flow 34 (2), 111–127.
Hewitt, G.F., Hall-Taylor, N., 1970. Annular Two-Phase Flow. Pergamon Press, Oxford.
Hewitt, G.F., Martin, C.J., Wilkes, N.S., 1985. Experimental and modelling studies of annular flow in the region between flow reversal and the pressure drop minimum. PhysicoChem. Hydrodyn. 6 (1/2), 69–86.
Holowach, M.J., Hochreiter, L.E., Cheung, F.B., 2002. A model for droplet entrainment in heated annular flow. Int. J. Heat Fluid Flow 23, 807–822.
Jayanti, S., Hewitt, G.F., 1992. Prediction of the slug-to-churn flow transition in vertical two-phase flow. Int. J. Multiph. Flow 18 (6), 847–860.
McQuillan, K.W., Whalley, P.B., Hewitt, G.F., 1985. Flooding in vertical two-phase flow. Int. J. Multiph. Flow 11 (6), 741–760.
Omebere-Iyari, N.K., Azzopardi, B.J., 2007. A study of flow patterns for gas/liquid flow in small diameter tubes. Chem. Eng. Res. Des. 85 (2), 180–192.
Owen, D.G., 1986. An Experimental and Theoretical Analysis of Equilibrium Annular Flows Ph.D. Thesis. University of Birmingham, UK.
Parsi, M., Vieira, R.E., Torres, C.F., et al., 2015a. On the effect of liquid viscosity on interfacial structures within churn flow: experimental study using wire mesh sensor. Chem. Eng. Sci. 130, 221–238.
Parsi, M., Vieira, R.E., Torres, C.F., et al., 2015b. Experimental investigation of interfacial structures within churn flow using a dual wire-mesh sensor. Int. J. Multiphase Flow, 155–170.
Parsi, M., Agrawal, M., Srinivasan, V., et al., 2016. Assessment of a hybrid CFD model for simulation of complex vertical upward gas–liquid churn flow. Chem. Eng. Res. Des. 105, 71–84.
Ryua, S.H., Park, G.C., 2011. A droplet entrainment model based on the force balance of an interfacial wave in two-phase annular flow. Nucl. Eng. Des. 241, 3890–3897.
Sawai, T., Kaji, M., Kasugai, T., et al., 2004. Gas–liquid interfacial structure and pressure drop characteristics of churn flow. Exp. Therm Fluid Sci. 28 (6), 597–606.
Sharaf, S., van der Meulen, G.P., Agunlejika, E.O., et al., 2016. Structures in gas–liquid churn flow in a large diameter vertical pipe. Int. J. Multiph. Flow 78, 88–103.
Shearer, C.J., Davidson, J.F., 1965. The investigation of a standing wave due to gas blowing upwards over a liquid film; its relation to flooding in wetted-wall columns. J. Fluid Mech. 22 (02), 321–335.
Tekavčič, M., Končar, B., Kljenak, I., 2016. Simulation of flooding waves in vertical churn flow. Nucl. Eng. Des. 299, 214–224.
Van Nimwegen, A.T., Portela, L.M., Henkes, R., 2015. The effect of surfactants on air–water annular and churn flow in vertical pipes. Part 2: Liquid holdup and pressure gradient dynamics. Int. J. Multiph. Flow 71, 146–158.
Waltrich, P.J., Falcone, G., Barbosa, J.R., 2013. Axial development of annular, churn and slug flows in a long vertical tube. Int. J. Multiph. Flow 57, 38–48.
Wang, Z., Gabriel, K.S., Manz, D.L., 2004. The influences of wave height on the interfacial friction in annular gas–liquid flow under normal and microgravity conditions. Int. J. Multiph. Flow 30 (10), 1193–1211.
Wang, K., Bai, B.F., Cui, J.H., Ma, W.M., 2012. A physical model for huge wave movement in gas-liquid churn flow. Chem. Eng. Sci. 79 (10), 19–28.
Wang, K., Bai, B.F., Ma, W.M., 2013a. Huge wave and drop entrainment mechanism in gas-liquid churn flow. Chem. Eng. Sci. 104, 638–646.
Wang, K., Bai, B.F., Ma, W.M., 2013b. A model for droplet entrainment in churn flow. Chem. Eng. Sci. 104, 1045–1055.